

SACLANTCEN MEMORANDUM  
serial no.: SM-248

*SACLANT UNDERSEA  
RESEARCH CENTRE*

*MEMORANDUM*



**A simple deconvolution  
method for NAPOLI '85**

**J.R. Potter**

**October 1991**

The SACLANT Undersea Research Centre provides the Supreme Allied Commander Atlantic (SACLANT) with scientific and technical assistance under the terms of its NATO charter, which entered into force on 1 February 1963. Without prejudice to this main task – and under the policy direction of SACLANT – the Centre also renders scientific and technical assistance to the individual NATO nations.

---

This document is released to a NATO Government at the direction of SACLANT Undersea Research Centre subject to the following conditions:

- The recipient NATO Government agrees to use its best endeavours to ensure that the information herein disclosed, whether or not it bears a security classification, is not dealt with in any manner (a) contrary to the intent of the provisions of the Charter of the Centre, or (b) prejudicial to the rights of the owner thereof to obtain patent, copyright, or other like statutory protection therefor.
- If the technical information was originally released to the Centre by a NATO Government subject to restrictions clearly marked on this document the recipient NATO Government agrees to use its best endeavours to abide by the terms of the restrictions so imposed by the releasing Government.

---

Page count for SM-248  
(excluding covers)

---

Pages	Total
i-iv	4
1-22	22
	<hr/> 26

---

SACLANT Undersea Research Centre  
Viale San Bartolomeo 400  
19026 San Bartolomeo (SP), Italy

tel: 0187 540 111  
fax: 0187 524 600  
telex: 271148 SACENT I

NORTH ATLANTIC TREATY ORGANIZATION

SACLANTCEN SM-248

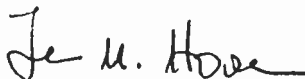
## A simple deconvolution method for NAPOLI '85

J.R. Potter

---

The content of this document pertains to work performed under Project 05 of the SACLANTCEN Programme of Work. The document has been approved for release by The Director, SACLANTCEN.

Issued by:  
Underwater Research Division



J.M. Hovem  
Division Chief



SACLANTCEN SM-248

**A simple deconvolution method for  
NAPOLI '85**

J.R. Potter

**Abstract:** An inverse filter (deconvolution in the frequency domain) is applied to acoustic results from the NAPOLI '85 experiment in order to obtain an estimate of the impulse response function of the medium. This method represents a very simple approach and requires few assumptions, making it robust to conceptual errors.

Signals were generated by small explosive charges and received at two hydrophone arrays placed at 500 m and 5000 m range from the source. To provide the impulse response function of the medium signals of the two hydrophone arrays were used in a deconvolution algorithm. The algorithm is described in detail and some measurement results are shown.

**Keywords:** deconvolution ◦ impulse response function ◦ inverse filter ◦ NAPOLI '85

## Contents

1. Introduction . . . . .	1
2. The inverse filter . . . . .	3
2.1. <i>Mathematical development</i> . . . . .	3
2.2. <i>Tailoring to the NAPOLI '85 experiment</i> . . . . .	4
2.3. <i>Tuning the performance</i> . . . . .	7
2.4. <i>Implementation and numerical testing</i> . . . . .	9
3. NAPOLI '85 data results . . . . .	12
3.1. <i>Single signal deconvolution</i> . . . . .	12
3.2. <i>Averages over many signals</i> . . . . .	13
4. Modelling the IRF . . . . .	15
4.1. <i>The simplest model, a single delta pulse</i> . . . . .	15
4.2. <i>Multiple arrivals</i> . . . . .	17
5. Conclusions . . . . .	21
References . . . . .	22

**Acknowledgment:** The author thanks Jack Ianniello and Jens Hovem who suggested many interesting ideas and avenues to explore throughout the course of this work. He would like to give special recognition to Andrew Cox, who worked for 3 months successfully applying an adapted E-M algorithm to NAPOLI '85 data.

## 1

## Introduction

The deconvolution technique presented in this memorandum has been developed to analyse acoustic data from NAPOLI '85, an ocean/acoustic experiment in the Tyrrhenian Sea. A description of the experiment and the acoustic pulse arrival-time results for a single refracted ray are described by Potter et al. [1]. Acoustic energy over (at least) the frequency range 25–3000 Hz was provided by small explosive charges. The intention was to record the signals at two hydrophone arrays placed at 500 and 5000 m range, then to deconvolve the two signals to provide the impulse response function (IRF) of the intervening medium. The ocean transfer function (OTF) is the frequency-space analogue of the IRF, and can be obtained by a fourier transform. We shall therefore only consider the IRF. The near and distant arrays consisted of 4 and 32 hydrophones, respectively. The acoustic geometry is shown in Fig. 1. The geometry was chosen as far as possible to allow energy travelling along a single macro-path, the lower refracted ray, to arrive at both arrays at a time well separated from other paths, enabling other path energy to be gated out in the time domain. A low-pass filter was applied to the data at each hydrophone array before recording at 6 kHz sampling rate. The digital resolution of the recordings was 72 dB.

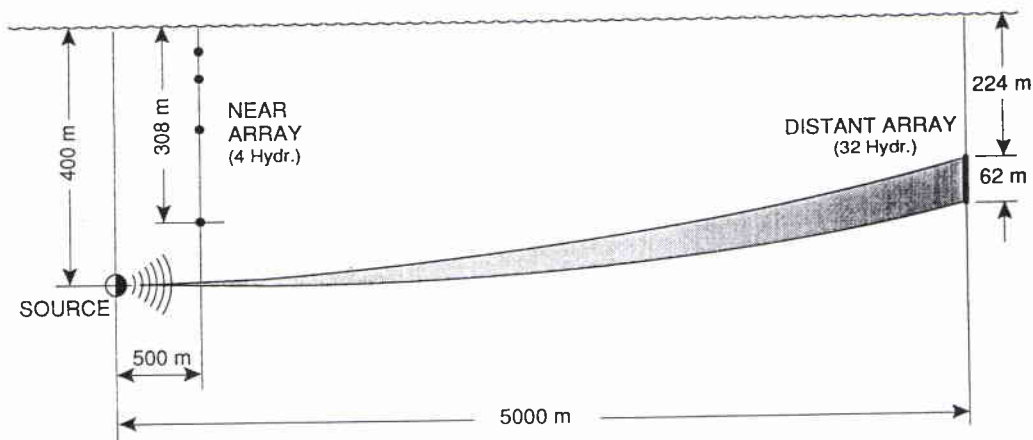
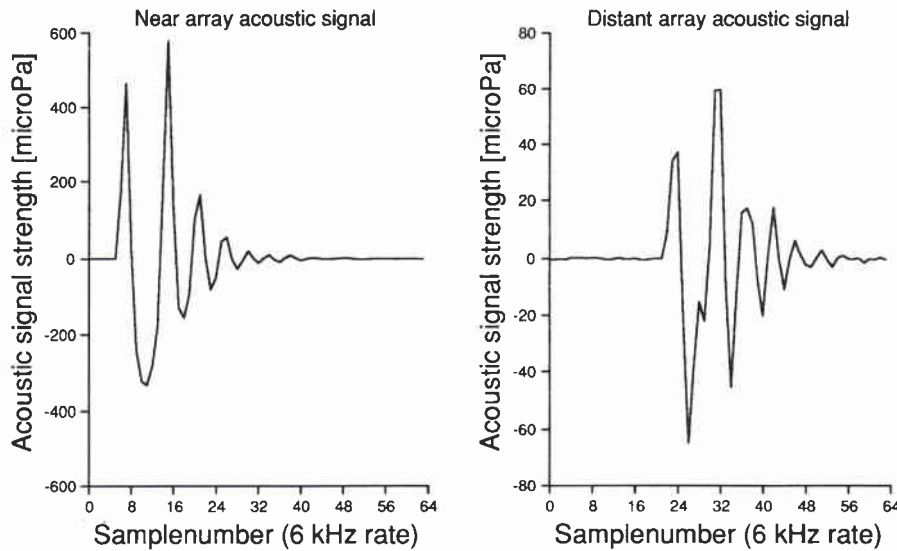


Figure 1 The geometry of the eigenpaths from source ship to distant array.

Some 196 signals were recorded on both hydrophone arrays over a period of 3 days. The acoustic intensity of signals arriving via the lower refracted path at the far-

ther array varied by some 3 dB rms, primarily due to variability in the intervening medium. The average signal-to-noise ratio over time, over the whole bandwidth, was some 40 dB. An example signal pair from the near array (left panel) and distant array (right panel) is shown in Fig. 2.

Event number 009, hydrophone number 02



**Figure 2** An example, from the first recorded event, of the near (left panel) and distant (right panel) recorded signals. Note the different vertical scales. These signals appear of quite different shape, due to the differences between  $M_n(f)$  and  $M_d(f)$ .

With such a high SNR, broadband signal, single-ray path, no boundary interaction and measured source signals rather than theoretical replicas, deconvolution should be relatively easy. Indeed, there are many techniques which can be applied to estimate the IRF. This memorandum shows that a very simple algorithm can be useful in providing robust and reliable (if coarse) estimates of the IRF. It appears that in the case of NAPOLI '85, a simple physical model is sufficient to extract almost all the available information.



## 2

## The inverse filter

We wish to develop a simple and robust algorithm that requires the least a-priori external information. The analysis developed here is little more than an application of the well-known inverse filter such as described by Hovem [2]. The analysis is repeated here for completeness, because it is short and because there are some details specific to the NAPOLI '85 dataset.

## 2.1. MATHEMATICAL DEVELOPMENT

We wish to investigate how a transmitted broadband signal propagates from a position **P** to **Q** in the ocean medium, imposing the minimum a-priori physical conditions, to keep the number of assumptions as few as possible. We begin by proposing a linear model for energy propagating along the eigenray(s) from **P** to **Q** so that the continuous time signal  $q(t)$  of this energy at position **Q** can be represented as a linear function of the continuous time signal  $p(t)$  at position **P**:

$$q(t) = i(t) * p(t), \quad (1)$$

where  $i(t)$  will be called the impulse response function (IRF) of the medium between **P** and **Q** and the asterisk indicates the convolution integral. What we measure with our hydrophones are not  $p(t)$  and  $q(t)$  but these signals plus noise (defined as energy which arrives at **P** and **Q** but which does not propagate along the eigenray(s) joining **P** and **Q**). In addition, we can see from Fig. 1 that even the deepest of the near-array hydrophones is significantly above the eigenrays from source to the distant array. We include this by introducing an error function  $e(t)$  such that  $e(t) * \hat{p}(t) = p(t)$ , where  $\hat{p}(t)$  is measured at the hydrophone nearest the eigenray and  $p(t)$  is the signal at the nearest point on the eigenray. We then obtain an expression for what we are able to measure:

$$q(t) + n_1(t) = i(t) * e(t) * [\hat{p}(t) + n_2(t)] + [n_1(t) - i(t) * n_2(t) * e(t)], \quad (2)$$

where  $n_1(t)$  and  $n_2(t)$  are noise contributions at **Q** and on the eigenray near **P**, respectively. Combining noise terms we obtain

$$r(t) = i(t) * e(t) * s(t) + n(t), \quad (3)$$

where  $r(t)$  and  $s(t)$  are the signals plus noise observed at **Q** and **P**, respectively. Taking the continuous fourier transform (FT) of Eq. (3) and using the linearity of

the FT and the convolution theorem gives

$$R(f) = I(f) \cdot E(f) \cdot S(f) + N(f), \quad (4)$$

where the uppercase letters indicate the FT partners of their lowercase counterparts and the dot indicates multiplication. Re-arranged this gives

$$I(f) = [R(f)/S(f)] \cdot [1 - N(f)/R(f)]/E(f), \quad (5)$$

providing  $S(f), E(f) \neq 0$ . We then solve for  $i(t)$  by taking the inverse FT.

## 2.2. TAILORING TO THE NAPOLI '85 EXPERIMENT

We must first guarantee  $S(f) \neq 0$  for our data. The signal source  $p(t)$  was produced by a small explosive charge, which is known to provide significant energy at least over the range  $25 < f < 3000$  Hz, so that  $S(f)$  is guaranteed non-zero at least over this frequency range. Values below 25 Hz are not of interest, resulting only in a quasi-DC component over the length of the signal (some 6 ms long).

Secondly, we note that  $s(t)$  and  $r(t)$  the signals arriving at the two hydrophone arrays may be subject to different pre-processing in the hardware of the two receiving and recording systems. We express the sum of these system effects in the near array as a function  $M_n(f)$  such that  $S'(f) = S(f) \cdot M_n(f)$ , where  $S'(f)$  is the filtered and recorded signal. It is easy to see that these effects would nearly cancel in Eq. (5) if  $R'(f) = R(f) \cdot M_n(f)$ ; i.e. if the distant array had the same anti-aliasing filter and associated electronics as the near array. Initially this was thought to be so. The deconvolution results thus obtained were inconsistent with expectations and, in the search for the problem, the near and distant arrays were re-calibrated in the SACLANTCEN tank facility.

Re-calibration revealed that the anti-aliasing filters in the two arrays differ in a way which becomes more acute at higher frequencies. The measured  $M_n(f)$  (for the near array) and  $M_d(f)$  (for one hydrophone of the distant array) are shown in Fig. 3. The accuracy of the amplitude calibrations together with the inter-hydrophone dependence is claimed to be within  $\pm 0.5$  dB. We might reasonably take this value to represent the  $2\sigma$  probability of a gaussian distribution of errors, indicating  $\sigma \simeq 3\%$ . The error in  $M_n(f)$  is likely to become larger for frequencies greater than 2.55 kHz, where the values have been extrapolated.

Finally, there are then two approximations to be made to Eq. (5) before application to the NAPOLI '85 data.

1.  **$N(f)$  is unknown.** To begin with, we make the simplest assumption that  $N(f) \ll R(f)$  (high SNR) so that  $[1 - N(f)/R(f)] \sim 1$ . Estimates of  $N(f)$  (from data recorded immediately before the explosive signal was fired) shows that the

SACLANTCEN SM-248

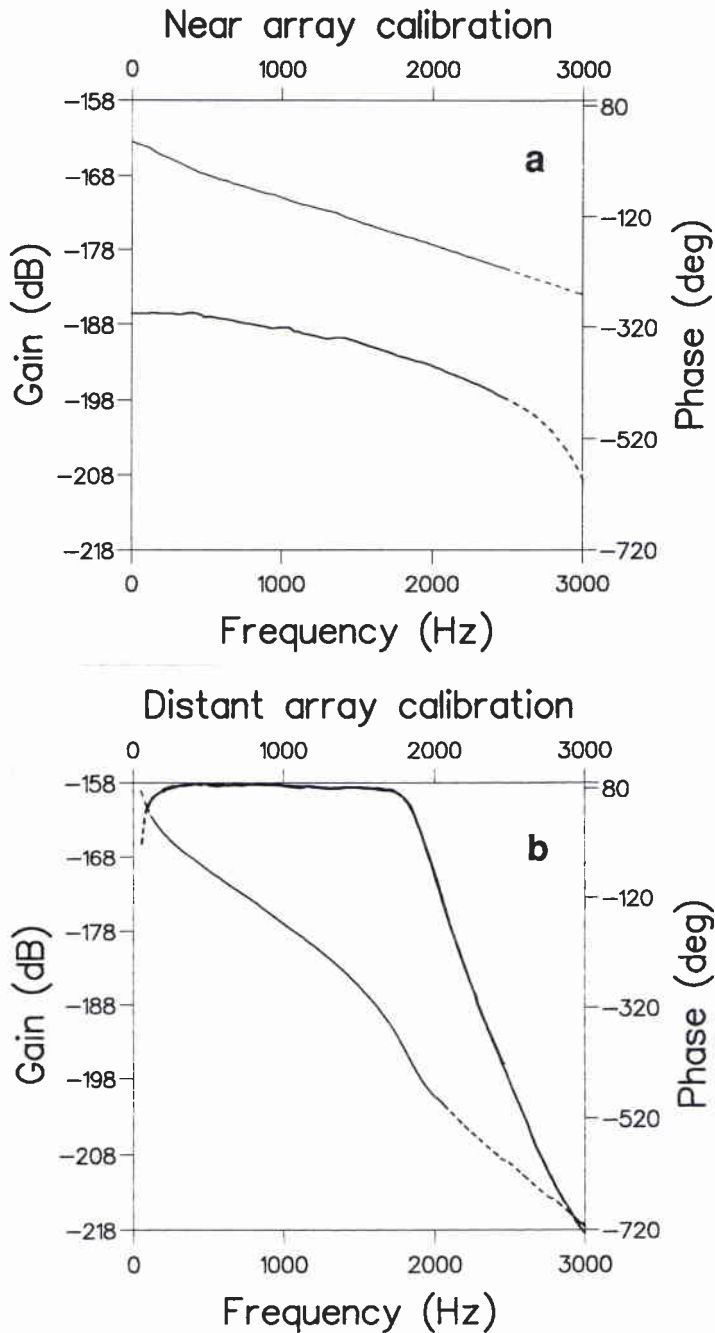


**Figure 3** The calibration curves for the near (a) and distant (b) arrays. The amplitudes are shown as the heavy lines, phases as light lines. Measured calibration values were not obtained for all frequencies from 0–3 kHz. Extrapolated values are shown dashed.

noise is nearly white over  $|f| \leq 3$  kHz, with  $N(f) \sim O(10^{-2}) \cdot R(f)$  for  $25 < f \leq 3$  kHz. Conservation of energy and horizontal isotropy indicates that  $I(f) \sim O(10^{-1})$ , so that  $N(f) \ll R(f) \ll S(f)$ . The error introduced by this approximation will then arise principally from the noise in  $r(t)$  and causes an error of  $\sim \pm 1\%$  in  $i'(t)$ , providing the noise is incoherent with  $r(t)$ . Since

the noise, by definition, does not travel along the eigenray(s), it cannot (in general) be coherent with  $r(t)$ . Any remaining doubt about ‘freak’ events can be removed by taking the average  $\bar{r}'(t)$  over many signals. We may therefore approximate  $N(f) = 0$ .

2.  $E(f)$  is unknown. We note that the signal traveling along the eigenray to the distant array has traversed 500 m horizontally and a negligible distance vertically at its nearest point of approach to the near array. The eigenray to the near array has a similar horizontal displacement, and 92-m vertical displacement. The horizontal length scale of sound-speed inhomogeneities at this depth has been estimated at between 2–6 km and the vertical scale is some 40–68 m [1,3] (depending on definition), so there is no multiple scattering and we expect no focusing or significant pulse spreading in such a short range. In addition, the two rays spend most of their travel-time close to each other, within the inhomogeneity scale. Only in the latter half of the 500-m path might they encounter a significantly different inhomogeneity. The dominant effect is a simple difference in arrival time, which is irrelevant to the deconvolution.

Results from the distant hydrophone array at **Q** indicate that signal intensities there vary by some  $\pm 3$  dB rms. If we make the first-order assumption that the variability can be accounted for by a smooth monotonic accretion of variability imposed by the sound-speed inhomogeneities, as for the relative arrival time (see Sect. 5.4 of [1]), we would expect some  $\pm 2\%$  error to be accrued in 250 m, the approximate distance that the two rays travel significantly separated. The error would be larger if there were some particularly strong feature between the source and **P** which affected the eigenray to **P** but not the eigenray to **Q**. The source ship drifted  $\pm 250$  m about its mean position with respect to **P** over the five days of the experiment during which some 72 XBT drops and 3 CTD casts were made. No such feature was observed at this depth. We conclude that the signals will have developed little significant modulation in such a short distance, and that even this modulation will be very little different from **P** to the adjacent eigenray. We may therefore approximate with small error  $E(f) \simeq 1$ .

With these approximations, we substitute into Eq. (5) to obtain the (very simple) result with  $I'(f)$  the estimated  $I(f)$ :

$$I'(f) = \begin{cases} [R'(f) \cdot M_n(f)]/[S'(f) \cdot M_d(f)], & |f| \leq 3 \text{ kHz} \\ 0, & |f| > 3 \text{ kHz}. \end{cases} \quad (6)$$

The analysis has so far been presented for the continuous case, whereas we have discrete data. This is resolved by invoking the sampling theorem, which guarantees that a continuous time series  $x(t)$  may be completely reconstructed from a regularly sampled time series  $x_i$  providing that  $X(f) = 0$  for all  $f > f_0$ , where  $f_0$  is half the sampling rate. Since our data were sampled at 6 kHz after low-pass filtering

the conditions for the theorem are satisfied. We may therefore guarantee that at any stage we can completely reconstruct, within error bounds and recorded dynamic range, the filtered continuous functions  $s'(t)$ ,  $r'(t)$ , and hence  $S'(f)$ ,  $R'(f)$ , from the discrete data. This was, of course, the motivation for the filtering in the first place.

### 2.3. TUNING THE PERFORMANCE

Equation (6) tells us how to obtain the estimate  $I'(f)$ , but not how this estimate is related to  $I(f)$ , i.e. how good an estimate is it? Since we estimate  $I'(f)$  only for  $f < f_0$  we may write

$$I'(f) = I(f) \cdot B(f), \quad (7)$$

where

$$B(f) = \begin{cases} 1, & |f| \leq f_0 \\ 0, & \text{otherwise,} \end{cases} \quad (8)$$

so that

$$i'(t) = i(t) * b(t). \quad (9)$$

It is a standard result that

$$b(t) = 2f_0 \cdot \sin(2\pi f_0 t) / (2\pi f_0 t), \quad (10)$$

which has a maximum at  $t = 0$  of  $2f_0$  and a minimum near  $t = \frac{3}{4}f_0$  of  $-0.42f_0$ . Normalising the inverse FT gives a peak value of 1.0 and a minimum value of  $-0.21$ . The half-width of  $b(t)$  (which gives a measure of the resolution of  $I'(t)$ ) is  $(2f_0)^{-1}$ .

We now introduce a physical model such that  $i(t)$  may be written as a sum of Dirac delta functions of amplitude  $a_j$  and time lag  $\tau_j$ :

$$i(t) = \sum_{j=1}^N a_j \cdot \delta(t - \tau_j). \quad (11)$$

If we do not require  $N$  to be finite, then it can be shown that this requirement presents no restrictions on  $i(t)$ . Substitution into Eq. (9) gives

$$i'(t) = \sum_{j=1}^N a_j \cdot b(t - \tau_j), \quad (12)$$

so that if, for example,  $i(t)$  consisted of one positive delta function (representing a single non-dispersive eigenray transmission), the  $i'(t)$  obtained from our data would behave like  $b(t)$ , rather than a delta function. We can suppress the sidelobes in our estimate  $i'(t)$  if we trade resolution.

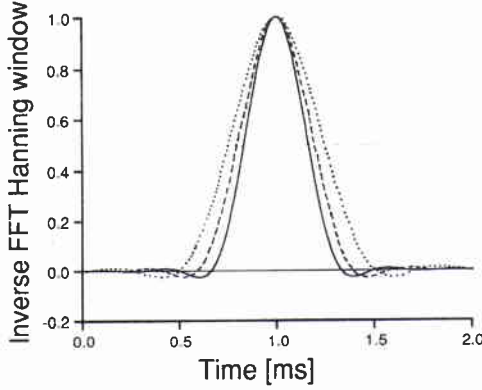


**Figure 4** The inverse FFT curves  $c(t)$ , for Hanning windows with  $f_0 = 2$  (solid line), 2.5 (dashed) and  $f_0 = 3$  kHz (dotted). The time axis has been stretched to highlight the peak broadening.

There are many possible choices for this filter. As is well known, sidelobe suppression (error reduction) is generally ‘paid for’ by a corresponding increase in the main lobe width (loss of resolution). It is clearly irrelevant to reduce the sidelobes below the level at which the error becomes noise-dominated. Our SNR is some 40 dB. Use of the Blackman window is therefore not justified, since it has a suppression of some 51 dB and would broaden the main lobe excessively. The Hamming window has the appropriate suppression, but the sidelobes are of nearly equal amplitude, which was thought undesirable. The Hanning window has a primary sidelobe suppression of 32 dB, with other sidelobes more strongly suppressed. The Hanning window was therefore chosen; this is defined by

$$C(f) = \begin{cases} \frac{1}{2} + \frac{1}{2} \cos(\pi f / f_0), & |f| \leq f_0 \\ 0, & \text{otherwise.} \end{cases} \quad (13)$$

Multiplying the  $I'(f)$  obtained from Eq. (6) by  $C(f)$  gives

$$\begin{aligned} I'(f) &= ([R'(f) \cdot M_n(f)] / [S'(f) \cdot M_d(f)]) \cdot B(f) \cdot C(f), \\ &= ([R'(f) \cdot M_n(f)] / [S'(f) \cdot M_d(f)]) \cdot C(f). \end{aligned} \quad (15)$$

The new estimated  $i'(t)$  then becomes

$$i'(t) = i(t) * c(t), \quad (16)$$

so that we can express  $i'(t)$  as

$$i'(t) = \sum_{j=1}^N a_j \cdot c(t - \tau_j). \quad (17)$$

Direct evaluation of  $c(t)$  from Eq. (14) shows that the primary sidelobes are 32 dB below the main peak, as expected. The sidelobe fall-off is 18 dB/octave band. Graphs of  $c(t)$  for  $f_0 = 2, 2.5$  and 3 kHz are shown in Fig. 4. The half-width of  $c(t)$  is  $f_0^{-1}$ , twice the half-width of  $b(t)$ . By using the Hanning window, we have traded resolution for accuracy.

SACLANTCEN SM-248

There remains one further concern. The small values of  $S'(f)$  and  $R'(f)$  may give rise to instabilities at  $|f| \sim 0$  and  $f_0$ , especially when errors in the extrapolation of  $M_n(f)$  are included. The former gives rise to a quasi-constant error in the time domain, which is of no concern. A simple DC correction has been made to the estimated IRF's shown in this memorandum. The latter causes some high-frequency 'jitter'. Effectively, at frequencies near  $f_0$  we are dividing one very small number by another, and so the result becomes unstably sensitive to small errors. Such instability is suppressed by multiplication by  $C(f)$  which goes smoothly to zero at  $f_0$ . The concern that this may be insufficient may be allayed by using a Hanning filter with  $f_0 = 2.5$  instead of 3 kHz, which eliminates the instability at the cost of loss of bandwidth. Alternatively, averaging over many pulses also suppresses the effect of noise, but not of calibration error. We therefore conclude that the DC offset and high-frequency behaviour of single deconvolutions may be suspect, but that this can be cured if necessary by using  $f_0 = 2.5$  kHz instead of 3 kHz and is ameliorated by averaging over many signals.

#### 2.4. IMPLEMENTATION AND NUMERICAL TESTING

An inverse filter program was written (IF) to apply the algorithm of Eq. (15). Before applying IF to the NAPOLI '85 data, it seemed a simple and useful exercise to test it on simulated data. A program was developed to generate test data, with known  $i(t)$ , for input to the IF program to compare  $i'(t)$  with known  $i(t)$  as a check that the relationship in Eq. (16) holds, within expected errors. Where the data input is obtained from a known  $i(t)$  (test data),  $i'(t)$  was evaluated from Eq.(16) and was plotted together with the  $i'(t)$  calculated by the IF program for comparison.

The test data were created by the following steps:

- An example signal  $s(t)$  recorded at the near array was read in and 64 data samples taken around the signal, representing 10.7 ms of data.
- An FFT was applied and a randomised error of 3.6% added to simulate the combined effects of  $E(f)$  and calibration errors, then an inverse FFT was applied.
- The signal was interpolated by a factor of 20 to simulate the continuous signal. Interpolation is not strictly necessary, but allows replicas of the signal to be inserted into the test data at times which are not whole multiples of the sampling period. When re-sampled, the simulated data (even if constructed from one delta function  $i(t)$ ) will in general have a different sampling phase from the source signal, as for real data.
- An amplitude and lag ( $a_j$  and  $t_j$  of Eq. (11)) were read in and a copy of the interpolated  $s(t)$  with amplitude  $a_j$  at time  $t_j$  was added to the test data. This step was repeated until all amplitudes and lags had been read from the specification file.

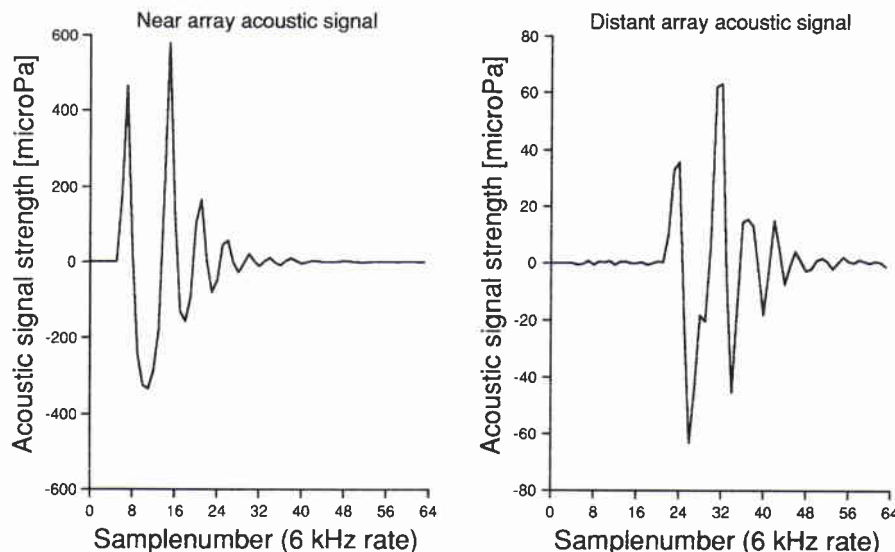


**Figure 5** The input signal  $s(t)$  from event 9 (lefthand panel) and the simulated received pulse  $r(t)$  (righthand panel), using a single delta pulse IRF. The pulse appears almost identical to the real data shown in Fig. 2.

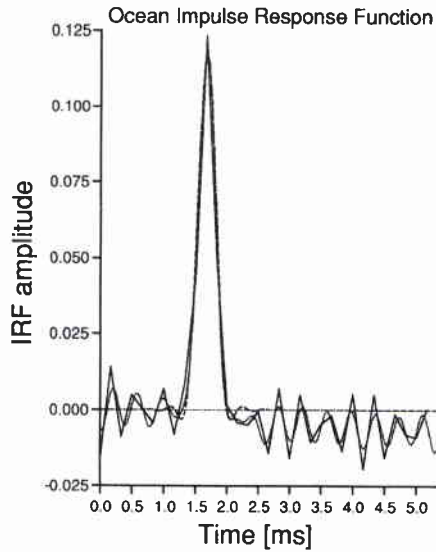
- The test data were sub-sampled at 6 kHz.
- White noise (1%) was added, consistent with the observed SNR.
- The test data were written to an output file with the same format as NAPOLI '85 data so that it could be used directly as input to the IF program.

The first test was to simulate data from a single delta pulse, to ensure that the IF program agreed with the prediction of Eq. (16) at least for the simplest case. The input signal  $s(t)$  was that of event 9 and is shown again in the lefthand panel of Fig. 5. The simulated distant signal  $r'(t)$  was obtained by simulating a pulse of amplitude 0.117 and is shown in the righthand panel of Fig. 5. The simulated  $r'(t)$  is strikingly similar to the real data  $r(t)$  shown in the righthand panel of Fig. 2, indeed almost identical. It is clear that the apparent differences in  $s(t)$  and  $r(t)$  are due to  $M_n(f)$  and  $M_d(f)$ , since the simulated data is able to recreate these differences using only a single delta pulse IRF. The estimated  $i'(t)$  and the function predicted from Eq. (16) for this case are shown in Fig. 6. Near the peak the agreement is excellent. Away from the peak the theoretical curve is zero but the estimated IRF fluctuates due to noise in the simulated data.

Further tests were conducted to synthesise data from a number of positive and negative delta pulses to demonstrate the most general case. In all cases the  $i'(t)$  calculated by the IF program and evaluated from Eq. (16) agreed within expected error limits.

In conclusion, we have developed a simple algorithm for estimating the IRF with



SACLANTCEN SM-248

**Figure 6** *The IRF for simulated data, estimated by the IF program with  $f_0 = 3$  kHz, shown as a solid line. The dotted line is a low-pass interpolated version. The theoretical IRF, calculated from Eq. (16), is shown dashed.*

a time resolution of 0.33 ms. The true widths of peaks in the IRF are correctly estimated, providing they exceed the resolution. Otherwise, the widths cannot be estimated except by a-priori assumptions about the physical process which give rise to the observed IRF. The errors introduced by the approximations of negligible noise ( $\pm 1\%$ ), the distortion  $E(t)$  ( $\pm 2\%$ ) together with hydrophone calibration uncertainties ( $\pm 3\%$ ) and sidelobes of the Hanning frequency filter ( $\pm 3\%$ ) result in an expected incoherent rms cumulative error of some  $\pm 5\%$ .

# 3

## NAPOLI '85 data results

---

The IF program runs quickly, requiring some 0.5 s or less on a VAX 8600 to estimate the IRF for 10 ms of data from a single hydrophone. With some 196 signals and 26 working distant hydrophones, this requires a total time of 40 CPU minutes to process the experimental data for one ray path. The IF program has also been run on the surface-interacting ray path signals. Ray-tracing indicates that the surface-interacting signal should contain a barely resolvable pair of rays, one reflected and one refracted.

For the purposes of this memorandum, we shall restrict ourselves to the results from the lower refracted path, which is expected to contain only one, non-surface-interacting, non-refracting ray.

### 3.1. SINGLE SIGNAL DECONVOLUTION

The IF program was applied to the signals shown in Fig. 2 with  $f_0 = 3$  kHz. The estimated IRF is shown in Fig. 7a and is very similar to the function  $c(t)$  with noise, and to the simulated data in Fig. 6. This is consistent with the expectation (from ray theory) that the true IRF is a single positive delta pulse. Figure 7 shows the high-frequency noise introduced by uncertainties near 3 kHz. In order to suppress this, the IF program was run on the same data with  $f_0 = 2.5$  kHz. The result is shown in Fig. 7b. The central peak is slightly broader and the background noise considerably less, as expected.

The IF program was run on many individual signal pairs, always with the same general result: that the IRF consists of a single peak of an amplitude consistent with ray-theory predictions and which appears very similar to the  $c(t)$  expected from a single pulse arrival.

## Event number 009, hydrophone number 02

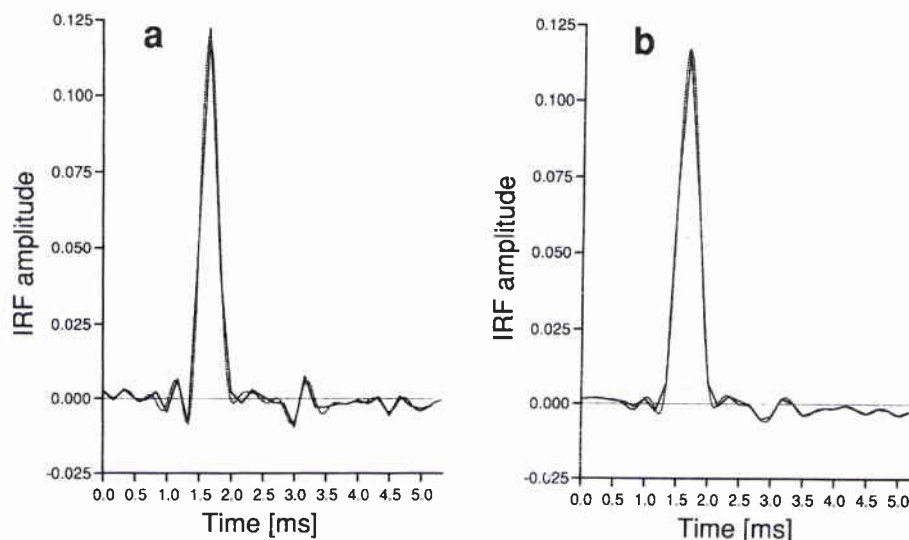


**Figure 7** The IRF estimated by the IF program with (a)  $f_0 = 3$  kHz and (b)  $f_0 = 2.5$  kHz for the data shown in Fig. 2. The solid line is the uninterpolated estimate, the dotted interpolated.

### 3.2. AVERAGES OVER MANY SIGNALS

In order to give some indication of time-variability the IF program was run on the first and last halves of the experiment, each consisting of over 2000 signals. The individual estimated IRF's in each case were averaged together, which should spread the estimated IRF peak if there is significant variability. In addition, the IF program was run on the entire experiment and averaged. Any noise contribution should average to very near zero over such a large number of signals, which spanned 3 days. The average  $i'(t)$  are shown for the entire, first half and second half of the experiment for  $f_0 = 3$  kHz in Figs. 8a–c. The averaged IRF's are both very similar to each other and to the IRF shown in Fig. 7 for one signal (with the expected suppression of high-frequency noise). The indication is that noise levels do not substantially alter the form of the pulse in single IRF estimates. While there may be amplitude variations of the IRF over the experimental period (indeed, the latter half has a significantly higher average amplitude than the first half), no significant shape (arrival-time structure) variations occur. This is consistent with expectations for the transmission range, centre frequency and low level of medium inhomogeneities encountered during the experiment.

One possibly significant feature is that all the average IRF's show some asymmetry around the main peak, suggesting the presence of a weak but persistent arrival structure other than a single pulse. This structure cannot be due to pulse spreading; rough-order calculations indicate spreading would be well below the resolution. The mechanism, although weak, must have a high temporal coherence for its effects on the IRF to be sustained throughout the experiment.

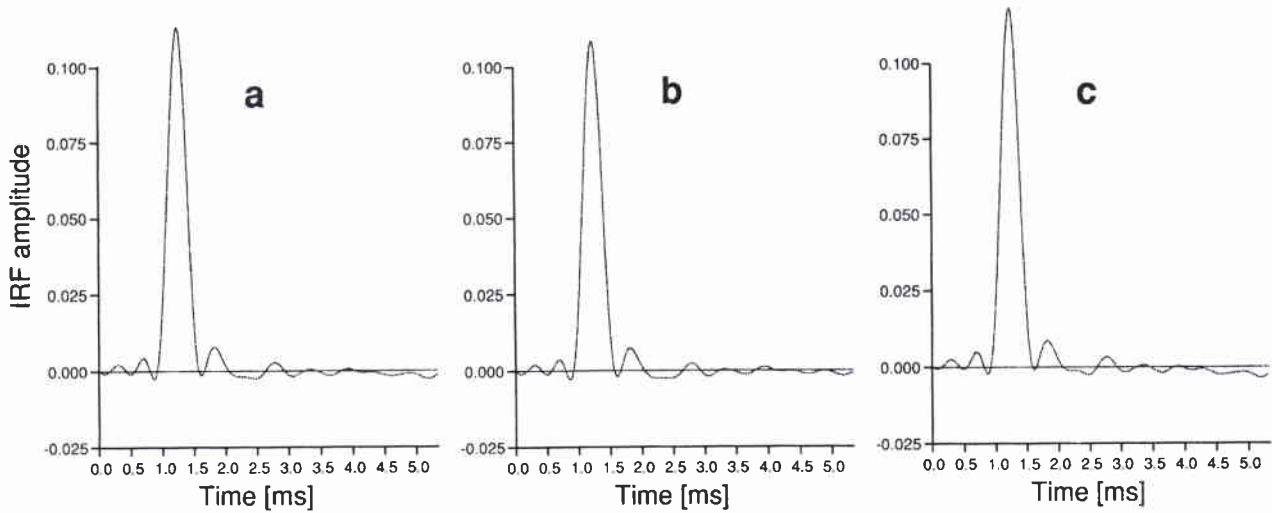


**Figure 8** (a) The estimated IRF, averaged over all the data (4820 signals) with  $f_0 = 3$  kHz. Individual IRF's were estimated by the IF program, then averaged by aligning the maximum interpolated value of each estimate to occur at a common time. (b) As for (a), but for only the first half of the experimental data (2540 signal pairs). (c) As for (a), but for the second half of the experimental data (2280 signal pairs).

## 4

## Modelling the IRF

Whilst the IF algorithm provides an estimate of the IRF, it does not provide an understanding of the physics of the system. As was noted from the results of the previous section, the estimated IRF is consistent with the simplest model of the IRF, that it is a single time-delayed, attenuated delta pulse. This is exactly the result expected from the simple geometry, short range and low-intensity sound-speed inhomogeneities encountered. Such a model incorporates assumed a-priori knowledge: that the true IRF will consist of an extremely narrow pulse. This pulse is expected to be far narrower than we can resolve with the bandwidth available in the NAPOLI '85 data.

## 4.1. THE SIMPLEST MODEL

We shall model the IRF by the simplest case of a single delta pulse. The estimate  $i'(t)$  then becomes  $= a_j \cdot \delta(t - \tau_j)$ ,  $j = 1$ , where  $a_j$  is the amplitude and  $\tau_j$  is the lag of Eq. (17) which we take as free parameters. The times measured at each array were not synchronised and so the observed travel-time to a single hydrophone yields no information. The amplitude is measured absolutely, and so this parameter can be compared with expectations. Ray-tracing indicates that the amplitude  $a_j$  should be  $\sim 0.11$ , with some variation due to the movement of the source ship. In order to calculate the absolute amplitude of the IRF, the effect of the source-ship movement nearer or farther from the arrays must obviously be taken into account.

The parameters of a single pulse arrival-time and amplitude were globally optimised by exhaustive search to minimise the normalised residual error variance  $NRE^2$  given by

$$NRE^2 = \sum_{i=0}^T \left[ r'(t_i) - \sum_{j=1}^N a_j \cdot s'(t_i - \tau_j) \right]^2 / \sum_{i=0}^T \left[ r'(t_i) \right]^2. \quad (19)$$

Equation (18) describes a commonly used cost parameter for measuring the 'skill' of an optimising algorithm. The minimisation of NRE results in the maximum likelihood estimate for the parameters. Figures 9a-c show the  $r'(t)$ ,  $i'(t) * s'(t)$  and the residual error obtained from this parameter optimisation for the bottom, centre and top hydrophones for event 9. The amplitude values obtained were 0.115, 0.108 and 0.114 respectively, in agreement with ray-tracing expectations. The residual errors

are shown in the righthand panels (note the change of axis scale). The NRE values were 7.9, 11.3 and 10.1% respectively, indicating that on average 90% of the signal  $r'(t)$  was accounted for by even this simplest of models. This is an extraordinarily good result.

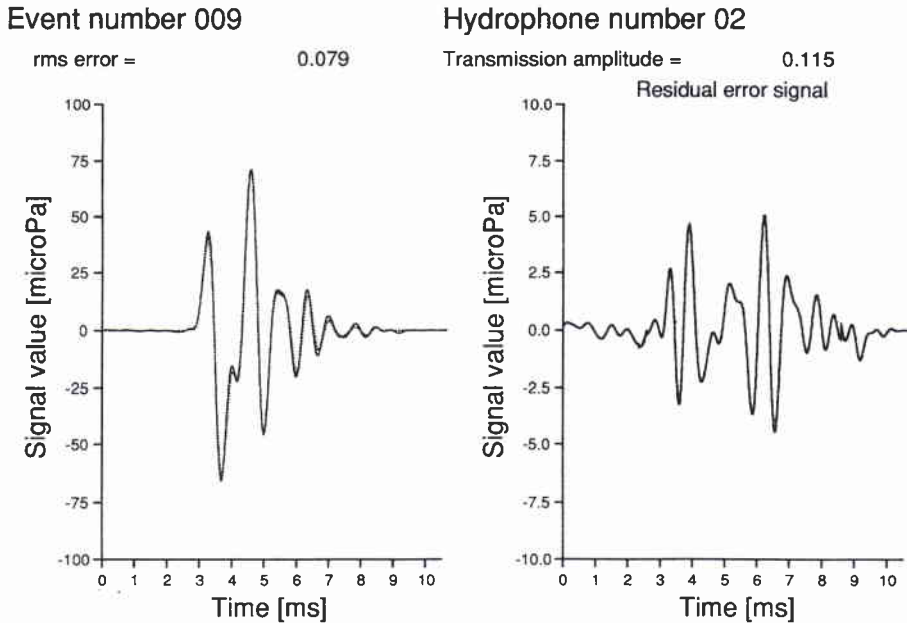


**Figure 9a** The lefthand panel shows the observed distant signal  $r(t)$  (solid line), and the predicted signal  $i'(t)*s(t)$  (dotted line) obtained from parameter optimisation of the simplest model of a single-pulse IRF for the bottom hydrophone of event 9. The residual error is shown in the righthand panel (note the vertical scale).

The parameter optimisation algorithm was applied to all the data, and the amplitude and residual error rms averaged over all satisfactory signals (some 1% of signals are degraded). The result over 4820 signals was a mean amplitude of 0.109 and a NRE of 9.9%. The indication is that the simplest model of a single-delta-pulse IRF explains nearly all of the available information in the recorded signal, over the entire experiment. The residual level may provide some additional information, but contains roughly equal proportions of information and noise.

SACLANTCEN SM-248

Event number 009

Hydrophone number 16

rms error = 0.113

Transmission amplitude = 0.108

Residual error signal

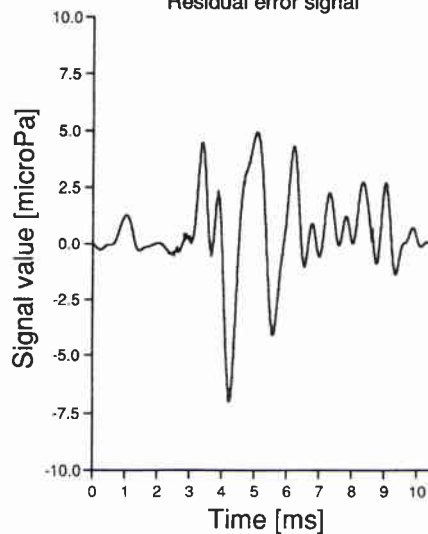
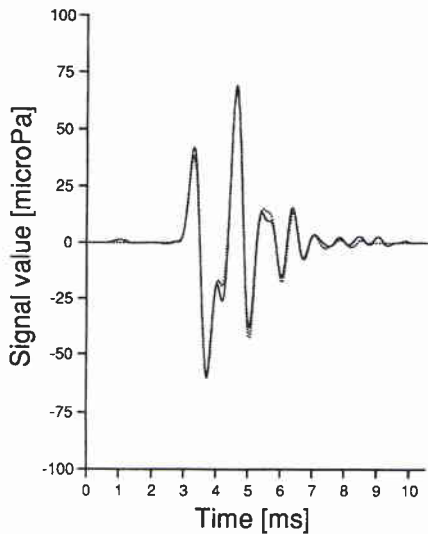


**Figure 9b** As Fig. 9a except for the centre hydrophone of event 9.

Event number 009

Hydrophone number 32

rms error = 0.101

Transmission amplitude = 0.114

Residual error signal

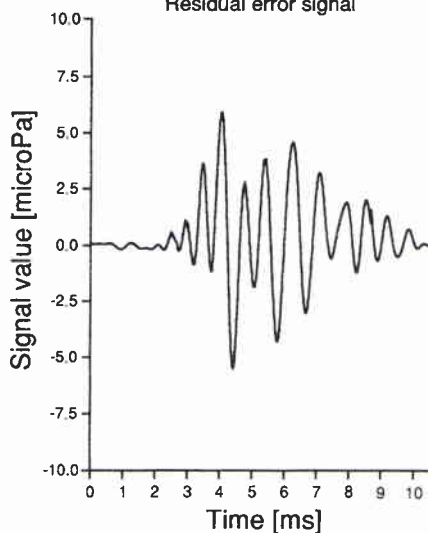
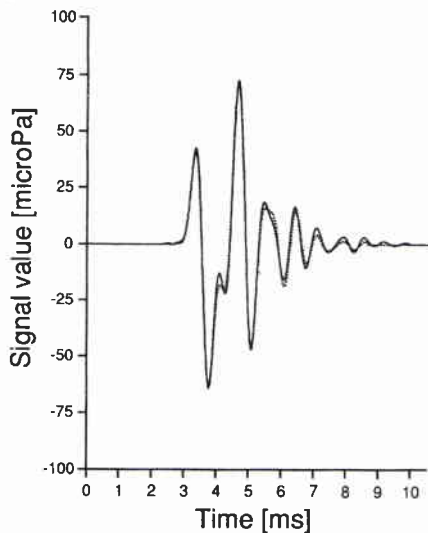


**Figure 9c** As Fig. 9a except for the top hydrophone.

#### 4.2. MULTIPLE ARRIVALS

The most obvious course of action to explore the little remaining information contained in the residual error is to allow the IRF to consist of more than one arrival. It seems reasonable to proceed by adding more pulses, one by one, observing how

the residual error reduces. The usual difficulty is to decide when to stop. Certainly, the addition of greater degrees of freedom is unwarranted if the NRE does not decrease correspondingly. One often-used criterion is to stop when the residual reduces to the noise level, or becomes white. Since the data is limited by calibration and other errors, rather than by noise, these indicators are inappropriate. It would be more reasonable to stop adding arrivals when the residual error no longer reduces appreciably and/or when the NRE closely approaches the expected minimum error of 4%.

The exhaustive parameter optimisation computation for more than one delta pulse rapidly becomes expensive. Ehrenberg et al. [4] showed that for  $N$  arrivals with parameters of lag and amplitude, the  $2N$  parameter search can be reduced to finding the maximum of the likelihood surface in an  $N$ -dimensional space. Even this rapidly becomes unwieldy and a sub-optimal optimisation such as the E-M algorithm [5] must be applied. For this memorandum, a simply adapted E-M algorithm was used to examine many arrival scenarios. The program, which we shall call estimate-maximise adapted (EMA), used the E-M algorithm of Feder and Weinstein [5] with three main differences:

The first adaptation was that arrivals were added singly between each estimation cycle, before maximising. The estimation was repeated if a pulse was added. The effect was to replace the estimation-maximising (E-M) cycle by an estimation-addition/estimation-maximise cycle until all allowed pulses had been placed. The algorithm was started with one pulse, at the matched correlator peak. This allowed the algorithm to quickly converge with one arrival to the dominant arrival feature, and to pick up remaining signals in order of importance. Secondly, further peaks were not introduced by randomly assuming some starting amplitude and lag, but by using the position and amplitude of the output from the matched-filter correlator run on the residual error. This provides a robust and simple first estimate which tends not to de-stabilise the algorithm. Thirdly, if any arrival amplitude falls below a threshold, chosen to be 0.0001 for this memorandum, it is removed.

We begin by examining the effect of allowing the IRF to consist of two arrivals. Three examples were calculated: the bottom, centre and top hydrophones for event 9. The EMA results are shown in Figs. 10a-c. In each case, the second arrival consists of a peak some 10-20 times smaller than the main peak, placed 0.49-0.67 ms afterwards. The NRE reduced to less than 7% in each case, very close to the expected optimum performance of 4%. It is not known if this pulse is an artifact of the equipment or an oceanic feature. It may be no more than a fortuitous coincidence that one extra pulse can explain, for the very limited number of three examples, most of the remaining information in the residual error.

The next step was to allow three arrivals. Again, the three examples for event 9 were chosen. Unsurprisingly, the EMA algorithm declined to place a third arrival for the top and bottom hydrophones. This indicates that no third arrival could be



SACLANTCEN SM-248

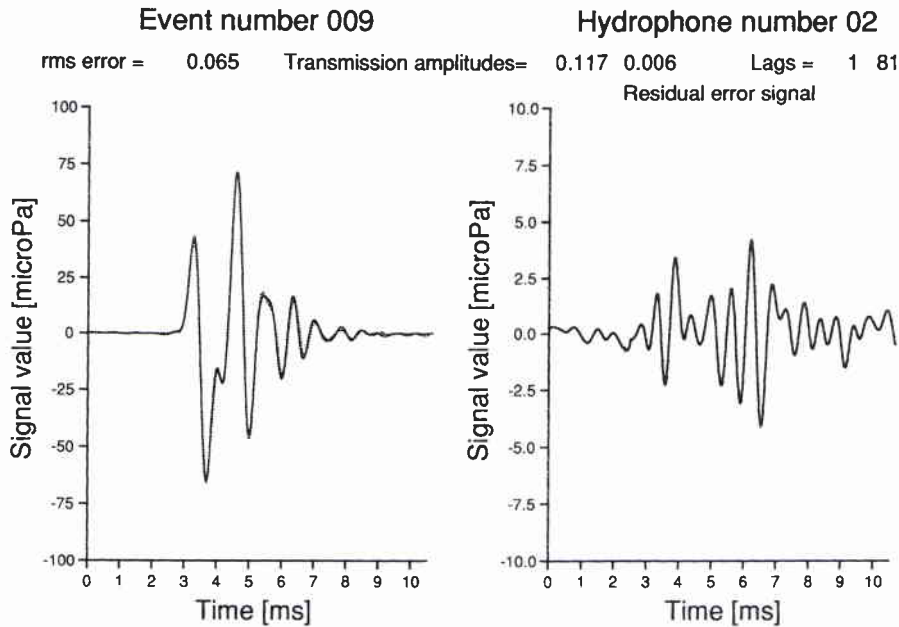


**Figure 10a** The lefthand panel shows the observed distant signal (solid line), and the predicted signal (dotted), obtained from the EMA algorithm for an IRF consisting of two pulses for the bottom hydrophone of event 9. The two lines are so close that they become indistinguishable over most of the signal. The residual error is shown in the righthand panel.

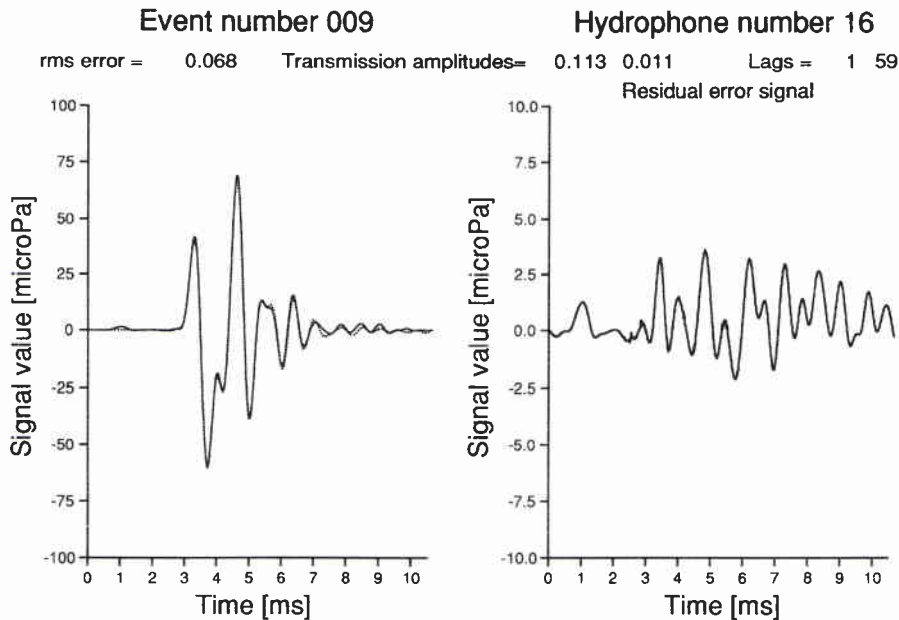


**Figure 10b** As Fig. 10a except for the centre hydrophone of event 9.

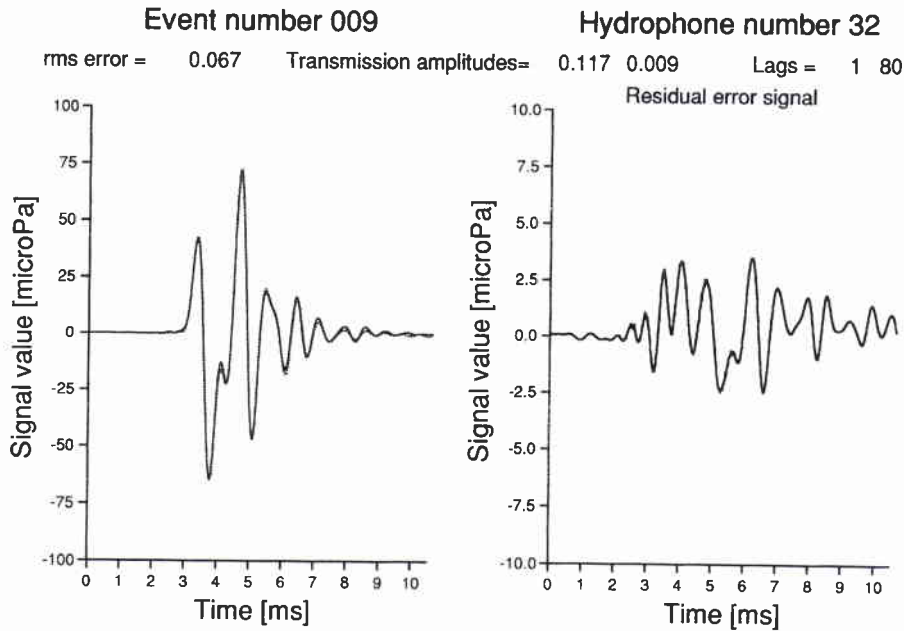


**Figure 10c** *As Fig. 10a except for the top hydrophone.*

found with an amplitude greater than 0.0001, corresponding to 60 dB below the main arrival amplitude. Clearly, allowing any number of arrivals greater than two has no effect on these signals. The centre hydrophone was fitted with a third peak of amplitude 0.004 (30 dB below the main peak) which was predicted to anticipate the main arrival by 0.1 ms. The third peak only reduced the NRE from 6.8 to 5.6%. Dashen et al. [6] showed that precursors do not occur unless there has been a caustic event. This result is then certainly spurious. The indication is that any more than two arrivals are superfluous, since the expected error of 4% is then almost reached and little improvement can be gained by additional pulses.

## 5

## Conclusions

---

The NAPOLI '85 acoustic data shows that the impulse response function for the lower refracted path is, to first order, a simple delayed delta pulse. The classical inverse filter can be applied with frequency filtering to reveal the essential features of the IRF. Pulse spreading is expected to be extremely small and, in any case, far below the resolution of the data given the available bandwidth. There is no indication of any significant changes in the shape of the IRF peak over the 3-day period of the experiment. Amplitude variations certainly occur. Multiple arrival structures are not observed, with the possible exception of a second pulse of amplitude less than one-tenth of the main arrival. The residual error obtained by fitting the simplest model IRF, a single delta pulse, is seen to be very small and approaches the expected error if two pulses are allowed. Given the very low residual error of the simplest IRF model, it is doubtful whether significant further information can be obtained by more complex algorithms.

## References

---

- [1] Potter, J.R., Akal, T. and Uscinski, B.J. Transmission-time variability, vertical spatial and temporal analysis of NAPOLI '85, an experiment in the Tyrrhenian Sea, SACLANTCEN SM-223. La Spezia, Italy, SACLANT Undersea Research Centre, 1989. [AD B 140 387]
- [2] Hovem, J.M. Removing the effect of the bubble pulses when using explosive charges in underwater acoustics experiment, SACLANTCEN TR-140. La Spezia, Italy, SACLANT Undersea Research Centre, 1969. [AD 849 890]
- [3] Potter, J.R. Oceanographic analysis of NAPOLI '85, an experiment in the Tyrrhenian Sea, SACLANTCEN SM-234. La Spezia, Italy, SACLANT Undersea Research Centre, 1990.
- [4] Ehrenberg, J.E., Ewart, T.E. and Morris, R.D. Signal-processing techniques for resolving individual pulses in a multipath signal. *Journal of the Acoustical Society of America*, **63**, 1978: 1861–1865.
- [5] Feder, M. and Weinstein, E. Parameter estimation of superimposed signals using the EM algorithm. *IEEE Transactions on Acoustics, Speech, and Signal Processing*, **36**, 1988: 477–489.
- [6] Dashen, R., Flatté, S.M. and Reynolds, S.A. Path-integral treatment of acoustic mutual coherence functions for rays in a sound channel. *Journal of the Acoustical Society of America*, **77**, 1985: 1716–1722.

### Initial Distribution for SM-248

#### SCNR for SACLANTCEN

SCNR Belgium	1
SCNR Canada	1
SCNR Denmark	1
SCNR Germany	1
SCNR Greece	1
SCNR Italy	1
SCNR Netherlands	1
SCNR Norway	1
SCNR Portugal	1
SCNR Spain	1
SCNR Turkey	1
SCNR UK	1
SCNR US	2
SECGEN Rep. SCNR	1
NAMILCOM Rep. SCNR	1

#### National Liaison Officers

NLO Canada	1
NLO Denmark	1
NLO Germany	1
NLO Italy	1
NLO Netherlands	1
NLO UK	1
NLO US	4
Total external distribution	26
SACLANTCEN Library	10
Stock	24
Total number of copies	60